Chinese Chemical Letters 35 (2024) 109639

Contents lists available at ScienceDirect

Chinese Chemical Letters

journal homepage: www.elsevier.com/locate/cclet

Efficient and selective photocatalytic nitrite reduction to N_2 through CO_2 anion radical by eco-friendly tartaric acid activation

Jingtai Bi[a,b], Yupeng Cheng[a], Mengmeng Sun[a,b,*], Xiaofu Guo[a,b], Shizhao Wang[a,b], Yingying Zhao[a,b,c,*]

[a] Engineering Research Center of Seawater Utilization of Ministry of Education, School of Chemical Engineering and Technology, Hebei University of Technology, Tianjin 300401, China
[b] Hebei Collaborative Innovation Center of Modern Marine Chemical Technology, Tianjin 300401, China
[c] Tianjin Key Laboratory of Chemical Process Safety, Tianjin 300130, China

ARTICLE INFO

Article history:
Received 20 October 2023
Revised 16 January 2024
Accepted 8 February 2024
Available online 13 February 2024

Keywords:
Nitrite
Advanced reduction processes
Photocatalysis
CO_2 anion radicals
Tartaric acid

ABSTRACT

In this study, the environmentally friendly precursor, tartaric acid (TA), was employed for the generation of CO_2 anion radical ($CO_2^{\bullet-}$) in an advanced UV/TA/Fe^{3+} system to reduce the hazardous NO_2^--N in wastewater. To optimize this process, various factors, including the dosage of Fe^{3+}, TA, and pH, were systematically investigated for their impact on the reduction process. Under the conditions of 3 mmol/L Fe^{3+} dosage, 10 mmol/L TA dosage, and a pH of 2.5, NO_2^--N was effectively removed from the water within 60 min, selectively transformed into N_2, with a remarkable N_2 selectivity of 91.2%. In the optimal conditions, the NO_2^--N reduction mechanism in the UV/TA/Fe^{3+} system and the critical role of $CO_2^{\bullet-}$ were illustrated. Finally, this study explored the reduction of real nitrified seawater using the UV/TA/Fe^{3+} system. The results demonstrated that the UV/TA/Fe^{3+} system could completely eliminate NO_2^--N and achieve a N_2 selectivity of up to 90%, with minimal interference from coexisting ions. This work holds promising implications for the environmentally benign treatment of nitrite-polluted wastewater.

The flue gas emitted by factories generates a large amount of wastewater containing nitrite, after undergoing denitrification process [1,2]. Nitrite poses significant risks to human health, as it can not only induce methemoglobinemia but also form potentially carcinogenic N-nitrosamines in the gastrointestinal tract [3,4]. In response to this situation, the World Health Organization (WHO) has set a limit of 3 mg/L for nitrite concentration in drinking water [5,6]. Therefore, to ensure the safety of drinking water, it is necessary to propose efficient methods to treat wastewater containing nitrite.

Currently, various methods are employed for the treatment of nitrite, including adsorption [7], membrane separation [8], biological approaches [9,10], electrochemical reduction [11,12], and photocatalytic reduction [13,14]. However, adsorption and membrane separation methods only concentrate nitrite without achieving its mineralization, which may result in potential secondary pollution. The biological method requires a relatively long period for cultivating adapted bacteria and mild conditions for microbial communities. The electrochemical method encounters challenges in the preparation of suitable electrocatalysts and the effective modulation of reduction products. In contrast, with the development of advanced reduction processes (ARPs), photocatalytic reduction has gained increasing popularity as an emerging approach for nitrite removal [15].

Photocatalytic reduction is an innovative and sustainable technology specifically developed for the treatment of oxidative pollutants in wastewater [16,17]. It utilizes electrons and highly reactive radicals generated under illumination to eliminate contaminants [18]. Among the various reductive radicals such as sulphur dioxide radical ($SO_2^{\bullet-}$) and bisulphide ion ($HS^{\bullet-}$) [19], $CO_2^{\bullet-}$ is a relatively emerging species [20,21]. It exhibits remarkable reducing capabilities by utilizing its unpaired electrons as electron donors. Hence, it possesses a strong reduction potential ($E^0(CO_2/CO_2^{\bullet-}) = -1.81$ V *vs.* SHE) and thus could effectively eliminate nitrite [22,23]. Numerous researchers have demonstrated that the reduction of NO_2^- by the $CO_2^{\bullet-}$ radical results in a high selectivity for N_2 in the resulting products [24]. Consequently, the primary products of the NO_2^- reduction in this process are N_2 and CO_2, mitigating the risk of secondary pollution compared to sulfur-containing radicals. However, this photocatalytic reduction process is limited by the $CO_2^{\bullet-}$

* Corresponding authors.
E-mail addresses: mengmeng_sun@hebut.edu.cn (M. Sun), luckyzhaoyy@126.com (Y. Zhao).

https://doi.org/10.1016/j.cclet.2024.109639
1001-8417/

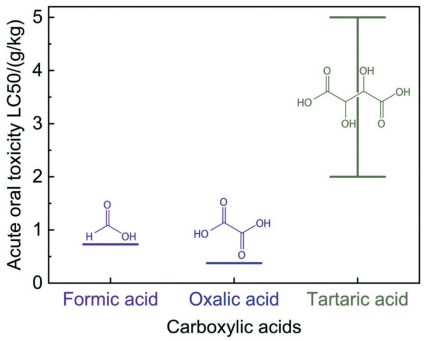

Fig. 1. Acute oral toxicity of carboxylic acids.

generated from the activation of carboxylic acid precursors [21,22]. Consequently, enhancing the efficiency and sustainability of $CO_2^{\bullet-}$ generation from these acids plays a significant role in modulating nitrite reduction [25]. As shown in Fig. 1, the group of common small molecular carboxylic acids comprises formic acid (FA), oxalic acid (OA), and TA. Considering the structural and property aspects of carboxylic acids, TA presents distinct advantages. Primarily, TA demonstrates heightened reducibility and possesses two carboxyl groups, potentially yielding a greater number of $CO_2^{\bullet-}$ during activation. Furthermore, with lower toxicity (Fig. 1), TA exhibits an acute oral toxicity LC_{50} value ranging from 2000 mg/kg to 5000 mg/kg (rat), significantly exceeding the values of formic acid (730 mg/kg) and oxalic acid (375 mg/kg), thereby signifying its reduced potential hazard [26]. Overall, TA serves as an effective and eco-friendly precursor for $CO_2^{\bullet-}$, highlighting its promising potential for application in the treatment of nitrite-containing wastewater.

To confirm the excellent characteristics of TA, a UV/Fe^{3+}/TA system was fabricated to explore the activation of TA in the production of $CO_2^{\bullet-}$ and the reduction of nitrite under various factors (Fe^{3+} dosage, TA dosage and pH). The details are shown in Supporting information.

In the UV/Fe^{3+}/TA system, Fe^{3+} primarily promotes the $CO_2^{\bullet-}$ activation from carboxylic acids through light-induced electron transfer and $^{\bullet}OH$ activation originating from its own photoactivity [25]. To examine the influence of Fe^{3+}, the impact of different Fe^{3+} dosage on the reduction of nitrite ions was investigated. As the Fe^{3+} dosage increases, the removal rate of NO_2^--N continuously rises, with pseudo-first-order rate constant increasing from 4.48 h^{-1} to 6.67 h^{-1}, suggesting that elevating the Fe^{3+} dosage can accelerate the reduction of NO_2^--N (Fig. 2a). As shown in Eqs. 1 and 2, upon exposure to ultraviolet light, Fe^{3+} engages in photoinduced electron transfer, facilitating the activation of TA to generate $CO_2^{\bullet-}$ and subsequently reducing the NO_2^- to form N_2 (Fig. 2b and Eq. 3). Consequently, increasing the Fe^{3+} dosage stimulates the production of $CO_2^{\bullet-}$, thereby boosting the reduction rate of NO_2^--N.

Except for the main product, N_2, there are three byproducts, namely NH_4^+-N, NO_3^--N, and NO_x, at the reaction endpoint under varying Fe^{3+} dosages, as shown in Fig. 2b. When the Fe^{3+} dosage is less than 4 mmol/L, the NH_4^+-N concentration remains negligible until the dosage reaches 5 mmol/L, producing around 1 mg N/L of NH_4^+-N. This effect arises due to the substantial generation of $CO_2^{\bullet-}$ at the 5 mmol/L dosage, causing an excessive reduction of NO_2^--N to NH_4^+-N. On the other hand, NO_3^--N demonstrates an initial decline followed by an increase on the graph. The minimum production of NO_3^--N is observed at a Fe^{3+} dosage of 3 mmol/L. This trend prompts speculation regarding the occurrence of reactions outlined in Eqs. 3 and 4. When subjected to ultraviolet light, Fe^{3+} undergoes self-photoreduction and generate $^{\bullet}OH$, which can activate TA to produce $CO_2^{\bullet-}$. Nevertheless, $^{\bullet}OH$ also exhibits potent oxidative characteristics, leading to the oxidation of NO_2^--N and the generation of NO_3^--N. Therefore, there is a trade-off effect between the accelerating generation of $CO_2^{\bullet-}$ and enhanced production of $^{\bullet}OH$ with the elevated Fe^{3+} undergoes, which induces the trend of NO_3^--N concentration exhibits as Fig. 2b. Specifically, with increasing Fe^{3+} dosage, the concentration of $CO_2^{\bullet-}$ rises. Simultaneously, the production of $^{\bullet}OH$ remains relatively low. Consequently, NO_2^--N mainly reacts with $CO_2^{\bullet-}$ to form N_2, and concurrently, oxidatively generated NO_3^--N can also undergo a reduction reaction with $CO_2^{\bullet-}$, resulting in a gradual decrease in the accumulation of NO_3^--N during the process. However, upon increasing the Fe^{3+} dosage to 4 mmol/L, the extent of Fe^{3+} photoreduction significantly increases, leading to a gradual rise in $^{\bullet}OH$ production. This phenomenon, in turn, leads to the accumulation of oxidatively formed NO_3^--N [24]. Consequently, NO_3^--N exhibits an ascending trend in the system. Finally, concerning NO_x, its presence was not detected in the gas phase, indicating the absence of NO_x generation within this specific dosage range.

$$Fe^{3+} + TA + h\nu \rightarrow Fe^{2+} + CO_2^{\bullet-} + CO_2\uparrow + H_2O \quad (1)$$

$$2NO_2^- + 8H^+ + 6CO_2^{\bullet-} \rightarrow N_2\uparrow + 6CO_2\uparrow + 4H_2O \quad (2)$$

$$Fe^{3+} + H_2O + h\nu \rightarrow Fe^{2+} + H^+ + {}^{\bullet}OH \quad (3)$$

$$NO_2^- + {}^{\bullet}OH \rightarrow NO_3^- + H^+ \quad (4)$$

Based on the above data, the variation in N_2 selectivity with Fe^{3+} dosages is depicted in Fig. 2c. With the Fe^{3+} dosage increasing from 1 mmol/L to 3 mmol/L, the N_2 selectivity rises from 85.5% to 91.2%. Conversely, as the Fe^{3+} dosage further increases from 3 mmol/L to 5 mmol/L, the N_2 selectivity decreases from 91.2% to 82.4%. This trend parallels the variation tendencies of the nitrogen byproducts in Fig. 2b. It particularly aligns with the trend of NO_3^--N production, influenced by the trade-off effect. Through comprehensive analysis, it is evident that at a Fe^{3+} dosage of 3 mmol/L, the production of nitrogen byproducts is minimized, and the N_2 selectivity reaches its peak. Consequently, the Fe^{3+} dosage of 3 mmol/L is chosen as the optimal condition.

Except for the Fe^{3+} dosage, TA functions as a precursor for $CO_2^{\bullet-}$ generation in UV/Fe^{3+}/TA system and was considered as a key factor. As illustrated in Fig. 3a, an increase in TA dosage results in a significant improvement in the removal rate of NO_2^--N. This observation suggests that higher TA dosages can significantly enhance the generation rate of $CO_2^{\bullet-}$, consequently enhancing the reduction of NO_2^--N. Fig. 3b illustrates the concentrations of three byproducts with changing TA dosages. As shown in Fig. 3b, NO_3^--N exhibits the highest production as a byproduct at a TA dosage of 5 mmol/L. With an increase in TA dosage, the elevated production of $CO_2^{\bullet-}$ promotes the reduction of NO_3^--N, resulting in a reduction of its concentration. However, the photocatalytic Fe^{3+}-generated $^{\bullet}OH$ also facilitates the transformation of NO_2^--N into NO_3^--N, thus maintaining NO_3^--N at approximately 3–3.5 mg N/L at TA dosage ranging from 10 mmol/L to 40 mmol/L. Additionally, as the TA dosage increases to 30 mmol/L or higher, the system generates additional NH_4^+-N and NO_x, with their concentrations correspondingly increasing as TA dosage rises. This phenomenon could be attributed to the excessive reducing agents TA and $CO_2^{\bullet-}$ over-reducing NO_2^--N into NH_4^+-N or NO_x. Finally, according to Fig. 3c, at a TA dosage of 5 mmol/L, the N_2 selectivity is 79.9%. As the dosage increases to 10 mmol/L, the N_2 selectivity significantly rises to 91.2%. However, with continued dosage escalation, the N_2 selectivity gradually decreases. Consequently, a TA dosage of 10 mmol/L is selected as the optimal condition to investigate the impact of pH on the performance.

As illustrated in Fig. 4a, the reduction rate of NO_2^--N exhibits a decreasing trend as pH increases, especially, this value significantly

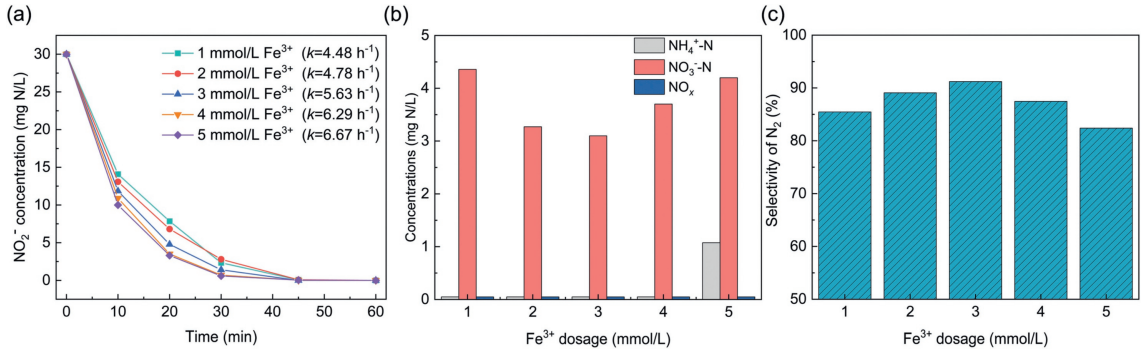

Fig. 2. Effect of Fe^{3+} dosage on (a) NO_2^--N degradation; (b) Concentrations of NH_4^+-N, NO_3^--N and NO_x at the reaction endpoint; (c) Selectivity of N_2. TA dosage: 10 mmol/L, pH 2.5.

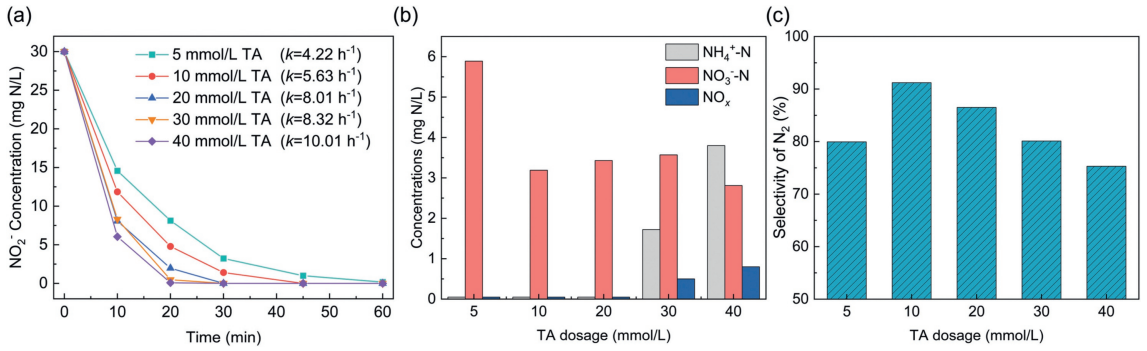

Fig. 3. Effect of TA dosage on (a) NO_2^--N degradation; (b) Concentrations of NH_4^+-N, NO_3^--N and NO_x at the reaction endpoint; (c) Selectivity of N_2. Fe^{3+} dosage: 3 mmol/L, pH 2.5.

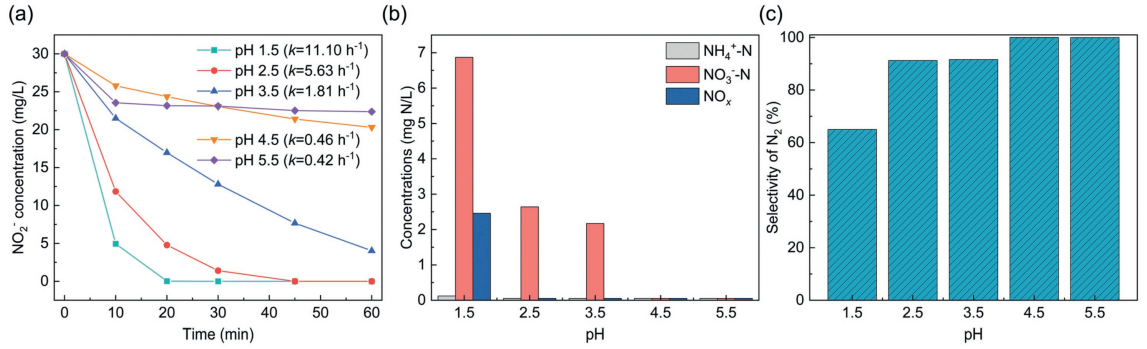

Fig. 4. Effect of pH on (a) NO_2^--N degradation; (b) Concentrations of NH_4^+-N, NO_3^--N and NO_x at the reaction endpoint; (c) Selectivity of N_2. Fe^{3+} dosage: 3 mmol/L, TA dosage: 10 mmol/L.

diminishes when pH ≥ 4.5. This is primarily because (1) the reduction of NO_2^--N requires lower pH levels to provide sufficient H^+ as proton to participate in the reaction, as shown in Eq. 2; (2) with increasing pH, the increasing OH^- precipitates Fe^{3+} into $Fe(OH)_3$ with lower photocatalytic activity. After the reduction reaction of NO_2^--N, the trends of three dominant byproducts are shown in Fig. 4b. It can be observed that when pH > 3.5, the byproduct concentrations are low. However, as the pH gradually decreases to 3.5 and below, the endpoint concentrations of NO_3^--N and NO_x significantly increase, while NH_4^+-N, although slightly elevated, remains at a relatively low concentration level. The occurrence of these phenomena may be attributed to the instability of trivalent NO_2^--N to the formation of NO_3^--N and NO by dimerization reactions under highly acidic conditions. Based on the above data, the N_2 selectivity was calculated, as illustrated in Fig. 4c. At a pH of 1.5, the prevalence of dimerization reactions results in the generation of a significant amount of NO_3^--N and NO_x, leading to lower N_2 selectivity. When the pH is increased, the photochemical reduction of NO_2^--N gains higher advantage over its inherent dimerization reaction, resulting in the higher N_2 selectivity. Considering the goal of efficiently treating harmful NO_2^--N, it was determined that under conditions of Fe^{3+} dosage at 3 mmol/L, TA dosage at 10 mmol/L, and pH at 2.5, it was possible to completely remove 30 mg N/L of NO_2^--N, with 91.2% of NO_2^--N being converted into N_2. However, the UV/TA/Fe^{3+} system also exhibits the ability to eliminate NO_2^--N at higher pH levels with satisfactory nitrogen selectivity. If the elimination rate of NO_2^--N is less favorable than the selectivity, a higher pH may also represent an optimal condition.

According to Section S3 in Supporting information, it can be concluded that only when UV, TA, and Fe^{3+} coexist, TA can be promptly activated to form $CO_2^{\bullet-}$, thus facilitating the efficient conversion of NO_2^--N to N_2. To further investigate the roles of the radicals in the mechanism, quenching experiments were conducted to confirm the presence and contributions of the related radicals. In

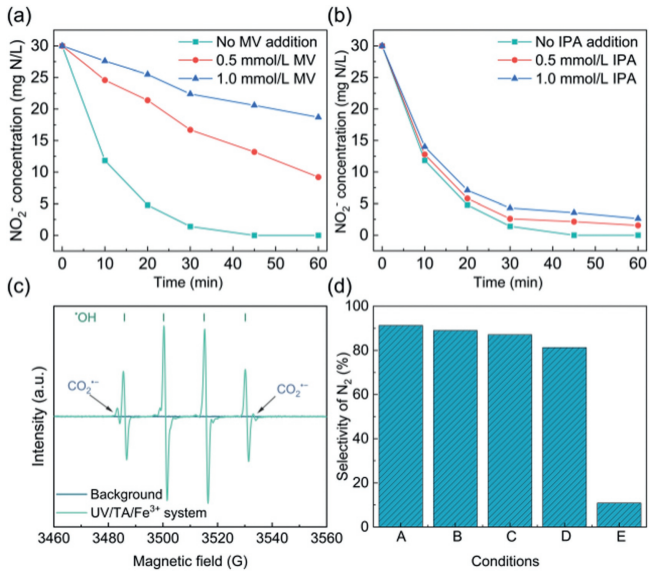

Fig. 5. Free radical quenching experiments: (a) NO_2^--N concentration in $CO_2^{\bullet-}$ quenching experiment; (b) NO_2^--N concentration in $^{\bullet}OH$ quenching experiment; (c) EPR free radical detection; (d) selectivity of N_2 in the presence of quenching agent (A: No quencher, B: 0.5 mmol/L IPA, C: 1.0 mmol/L IPA, D: 0.5 mmol/L MV, E: 1.0 mmol/L MV).

these experiments, methyl violet (MV) and isopropanol (IPA) were selected as quenchers for $CO_2^{\bullet-}$ and $^{\bullet}OH$, respectively [24]. Fig. 5a reveals a notable reduction in the efficiency of NO_2^--N degradation upon the addition of MV, indicating that $CO_2^{\bullet-}$ plays a dominant role as the key radical in NO_2^--N reduction. In contrast, the impact of IPA addition on NO_2^--N removal, as evident in Fig. 5b, appears comparatively limited, signifying that the activation of TA through the $^{\bullet}OH$ pathway is less potent compared to its direct activation by UV and Fe^{3+}. To provide additional clarity on the presence of these radicals, the electron paramagnetic resonance (EPR) technique was employed, utilizing DMPO as the spin-trapping agent. As depicted in Fig. 5c, the quadruplicate signal can be attributed to the DMPO-$^{\bullet}OH$ adducts, and the additional faint signals correspond to the DMPO-$CO_2^{\bullet-}$ [27]. Moreover, as illustrated in Fig. 5d, the influence of these two quenchers on N_2 selectivity becomes more evident. The addition of IPA results in a reduction of N_2 selectivity to approximately 87%, while the introduction of MV sharply decreases N_2 selectivity to around 11%. This observation underscores the predominant role of $CO_2^{\bullet-}$ in facilitating the successful reduction of NO_2^--N to N_2. Therefore, $CO_2^{\bullet-}$ stands as a critical radical determining whether NO_2^--N can be effectively and selectively reduced to N_2.

On the other hand, in the reduction mechanism, UV irradiation accompanied with Fe^{3+} would result in the decarboxylation of TA and the generation of $CO_2^{\bullet-}$ (Eq. 1). Accordingly, both Fe^{3+} and TA undergo transformations with the proceeding of NO_2^--N reduction. Fig. 6a illustrates the relationship between Fe^{3+}, Fe^{2+}, and the total iron ion concentration. Before the reduction of NO_2^--N, the total iron ion concentration matches that of Fe^{3+}, with no presence of Fe^{2+} in the solution system. As the reduction reaction progresses, the total iron ion content remains relatively constant, while the Fe^{3+} content gradually decreases, and the Fe^{2+} content increases. This indicates the conversion of Fe^{3+} to Fe^{2+} in the system, indicating that Fe^{3+} undergoes photoinduced electron transfer and photoreduction reactions, as described in Eqs. 1 and 3. Fig. 6b displays the variation in TOC concentration over time. As the reaction proceeds, TOC gradually decreases, signifying a reduction in the organic carbon content within TA. In conjunction with Fig. 6c, after UV irradiation, the carboxyl group intensity at 1264 cm^{-1} in the system is significantly lower compared to the TA and TA/Fe^{3+} groups, which further demonstrates that TA undergoes continuous decarboxylation and activation catalyzed by Fe^{3+} and UV [24]. Based on the HR-MS spectrum (Fig. S3 in Supporting information), the decarboxylation of TA may involve carboxylic intermediates such as oxalic acid and 2-oxoacetic acid, ultimately leading to the formation of $CO_2^{\bullet-}$. While HR-MS captured some of these intermediates, it is important to note that their concentrations are relatively low and most of the tartaric acid undergoes conversion to $CO_2^{\bullet-}$. These findings align with those presented in Fig. 6b, showing a decrease in TOC concentration in the UV/TA/Fe^{3+} system post-activation.

In summary, the reduction mechanism can be deduced as follows: Under UV irradiation, Fe^{3+} activates the carboxyl groups in TA through photoinduced electron transfer, generating $CO_2^{\bullet-}$ [24,28,29]. Additionally, Fe^{3+} undergoes photodegradation reactions in the presence of UV and produces $^{\bullet}OH$, which can also activate the carboxyl groups in TA to form $CO_2^{\bullet-}$ radicals [25]. However, it may also oxidize NO_2^--N into NO_3^--N [24]. Furthermore, TA can undergo self-photolysis under UV irradiation, albeit to a lesser extent. Once $CO_2^{\bullet-}$ is generated in the solution, it primarily reduces NO_2^--N to N_2, however, minor byproducts like NH_4^+-N, NO_3^--N, NO_x could also be undesirably generated due to excessive NO_2^--N reduction, dimerization reactions, and $^{\bullet}OH$ oxidation during the process [24,29].

According to the above discussions, the fabricated UV/TA/Fe^{3+} system efficiently reduces NO_2^--N to N_2. However, many real water bodies containing NO_2^--N are not simple single systems and their compositions are rather complex. Considering seawater as a potential flue gas absorption medium, it generates nitrified seawater containing NO_2^--N [30]. Thus, nitrified seawater serves as a typical real NO_2^--N pollution system. Therefore, we employ the UV/TA/Fe^{3+} system to assess its performance in treating real nitri-

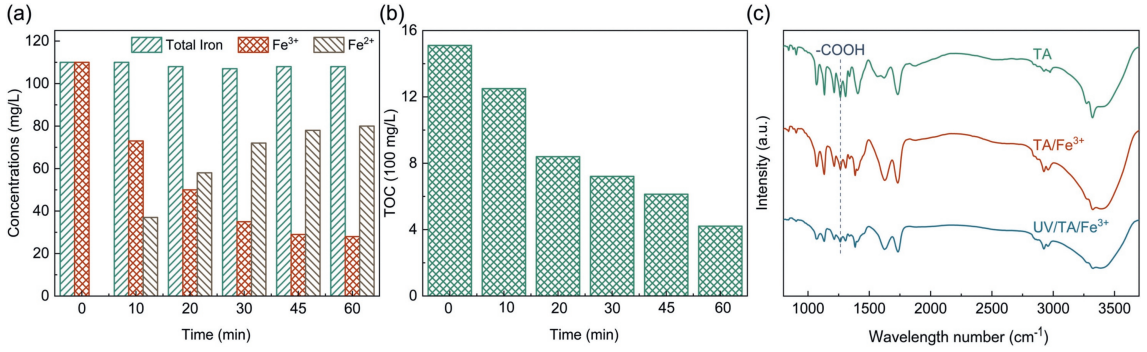

Fig. 6. (a) Concentration of iron species during reduction. (b) TOC concentration during reduction. (c) FTIR spectra of different systems.

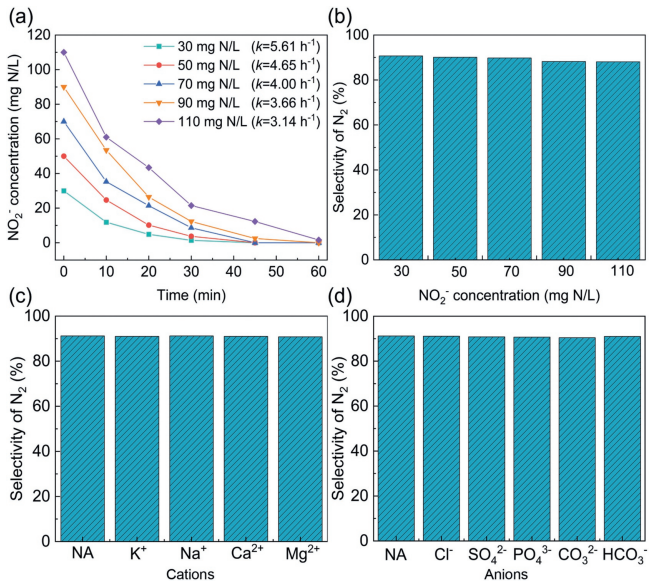

Fig. 7. (a) Effect of initial concentrations on NO_2^--N degradation in nitrified seawater. (b) Effect of initial concentrations on N_2 selectivity. (c) Effect of cations on N_2 selectivity. (d) Effect of anions on N_2 selectivity.

fied seawater. Table S1 (Supporting information) indicates the concentrations of ions other than NO_2^- in this water body.

As shown in Figs. 7a and b, at an initial NO_2^--N concentration of 30 mg N/L, the UV/TA/Fe^{3+} system rapidly removed NO_2^--N from nitrified seawater, achieving a N_2 selectivity of 90.7%, which is nearly identical to the optimal performance in aqueous solutions. To further confirm the efficiency of the UV/TA/Fe^{3+} system in treating real water samples, the influence of various ions present in seawater on the selectivity of NO_2^--N reduction was investigated. By introducing ions at concentrations consistent with those in nitrified seawater (Table S1 in Supporting information) in the aqueous system, as shown in Figs. 7c and d, it was observed that a range of common anionic and cationic species did not inhibit the reduction of NO_2^--N. This further substantiates the potential of the UV/TA/Fe^{3+} system in treating real wastewater. Furthermore, as the initial NO_2^--N concentration increased, the rate of NO_2^--N reduction in nitrified seawater gradually decreased from 5.61 h^{-1} at 30 mg N/L NO_2^--N to 3.14 h^{-1} at 110 mg N/L NO_2^--N. Nevertheless, as depicted in Fig. 7a, within the concentration range of 30–110 mg N/L NO_2^--N, the UV/TA/Fe^{3+} system effectively achieved complete removal of nitrites. Finally, Fig. 7b illustrates a slight decrease in N_2 selectivity with increasing initial NO_2^--N concentration. This primarily results from the reduction in $CO_2^{\bullet-}$ available per unit concentration of NO_2^--N as the NO_2^--N concentration rises, leading to reduced reduction efficiency.

In conclusion, this study proposes an eco-friendly approach employing TA as a precursor for nitrite reduction. Under the activation of Fe^{3+} and ultraviolet light, this system generates highly reducing $CO_2^{\bullet-}$ for selective reduction of nitrites to N_2. The impact of TA dosage, Fe^{3+} dosage and pH on the reduction process is systematically examined. The findings reveal that the UV/TA/Fe^{3+} system can completely eliminate nitrites from the wastewater within 1 h, achieving an impressive N_2 selectivity of 91.2%. Finally, this system is applied to the reduction of nitrites in nitrified seawater, demonstrating that even in complex seawater systems, nitrite removal is feasible, with N_2 selectivity consistently exceeding 90%.

Declaration of competing interest

The authors declare that they have no known competing financial interests or personal relationships that could have appeared to influence the work reported in this paper.

Acknowledgments

This research was financially supported by National Natural Science Foundation of China (No. 22208081), Central Guidance on Local Science and Technology Development Fund of Hebei Province (No. 226Z3102G) and Fundamental Research Funds of Hebei University of Technology (No. JBKYTD2001).

Supplementary materials

Supplementary material associated with this article can be found, in the online version, at doi:10.1016/j.cclet.2024.109639.

References

[1] X. Chen, X. Tong, J. Gao, et al., Environ. Sci. Technol. 56 (2022) 4542–4552.
[2] D.B. Gingerich, M.S. Mauter, Environ. Sci. Technol. 54 (2020) 3783–3792.
[3] C.P. Bondonno, L. Zhong, N.P. Bondonno, et al., Trends Food Sci. Technol. 135 (2023) 57–73.
[4] M. Carlström, C.H. Moretti, E. Weitzberg, J.O. Lundberg, Free Radic, Bio. Med. 161 (2020) 321–325.
[5] O. El hani, A. Karrat, K. Digua, A. Amine, Spectrochim. Acta A 267 (2022) 120574.
[6] H. Min, Z. Han, M. Wang, et al., Inorg. Chem. Front. 7 (2020) 3379–3385.
[7] M.R. Awual, M.M. Hasan, A. Islam, et al., J. Clean. Prod. 228 (2019) 778–785.
[8] X. Xiang, J. Wang, Q. Liu, et al., Sep. Purif. Technol. 275 (2021) 119195.
[9] M. Jiang, X. Zheng, Y. Chen, Water. Res. 169 (2020) 115242.
[10] B. Zhang, Y. Jiang, K. Zuo, et al., J. Hazard. Mater. 382 (2020) 121228.
[11] X. Zhang, Y. Wang, Y. Wang, et al., Chem. Commun. 58 (2022) 2777–2787.
[12] Y. Zhang, Y. Wang, L. Han, et al., Angew. Chem. Int. Ed. 62 (2023) e202213711.
[13] S.R. Huang, P.J. Huang, J. Environ. Chem. Eng. 10 (2022) 106902.
[14] S. Lee, Y. Lee, W. Choi, Appl. Catal. B 327 (2023) 122432.
[15] N. Hoinkis, M.I. Litter, Ind. Eng. Chem. Res. 61 (2022) 16408–16417.
[16] Q. Wang, L. Wang, S. Zheng, et al., J. Hazard. Mater. 451 (2023) 131149.
[17] J. Bi, X. Huang, J. Wang, et al., Chem. Eng. J. 366 (2019) 50–61.
[18] S. Lu, L. Shen, X. Li, et al., J. Clean. Prod. 378 (2022) 134589.
[19] X. Yu, D. Cabooter, R. Dewil, J. Hazard. Mater. 357 (2018) 81–88.
[20] C.M. Hendy, G.C. Smith, Z. Xu, T. Lian, N.T. Jui, J. Am. Chem. Soc. 143 (2021) 8987–8992.
[21] J. Guo, J. Deng, B. An, et al., Chemosphere 295 (2022) 133785.
[22] H. Shi, C. Li, L. Wang, et al., Sep. Purif. Technol. 300 (2022) 121854.
[23] S. Wang, Y. Zhao, J. Feng, et al., Chem. Eng. J. 455 (2023) 140787.
[24] B. An, H. He, B. Duan, J. Deng, Y. Liu, Chemosphere 278 (2021) 130388.
[25] B. Wang, B. An, Y. Liu, J. Chen, J. Zhou, Sep. Purif. Technol. 248 (2020) 117061.
[26] Merck Millipore, Safety data sheet.
[27] Q. Zhou, W. Niu, Y. Li, X. Li, J. Clean. Prod. 258 (2020) 120790.
[28] J. Chen, R. Zhang, D. Chen, J. Liu, S. Chen, J. Water Process Eng. 40 (2021) 101934.
[29] Z. Shi, F. Wang, Q. Xiao, S. Yu, X. Ji, Catalysts 12 (2022) 348.
[30] Y. Zhao, Y. Cheng, T. Zhang, et al., Fuel 340 (2023) 127436.